THE JOURNAL OF BIOLOGICAL CHEMISTRY VOL. 281, NO. 8, pp. 5026–5031, February 24, 2006

Solution Structure of the Human Ubiquitin-specific Protease 15 DUSP Domain*

Received for publication, October 7, 2005, and in revised form, November 17, 2005 Published, JBC Papers in Press, November 18, 2005, DOI 10.1074/jbc.M510993200

Rob N. de Jong[1], **Eiso AB**[1], **Tammo Diercks, Vincent Truffault**[2], **Mark Daniëls, Robert Kaptein, and Gert E. Folkers**[3]

From the Department of NMR Spectroscopy, Bijvoet Center for Biomolecular Research, Utrecht University, Padualaan 8, 3584 CH Utrecht, The Netherlands

Ubiquitin-specific proteases (USPs) can remove covalently attached ubiquitin moieties from target proteins and regulate both the stability and ubiquitin-signaling state of their substrates. All USPs contain a conserved catalytic domain surrounded by one or more subdomains, some of which contribute to target recognition. One such specific subdomain, the DUSP domain (domain present in ubiquitin-specific proteases), is present in at least seven different human USPs that regulate the stability of or interact with the hypoxia-inducible transcription factor HIF1-α, the Von Hippel-Lindau protein (pVHL), cullin E3 ligases, and BRCA2. We describe the NMR solution structure of the DUSP domain of human USP15, recently implicated in COP9 (constitutive photomorphogenic gene 9) -signalosome regulation. Its tripod-like structure consists of a 3-fold α-helical bundle supporting a triple-stranded anti-parallel β-sheet. The DUSP domain displays a novel fold, an α/β tripod (AB3). DUSP domain surface properties and previously described work suggest a potential role in protein/protein interaction or substrate recognition.

There are at least 67 human deubiquitinating enzymes, subdivided in ubiquitin-specific proteases (USPs)[4] and ubiquitin carboxyl-terminal hydrolases. By removing covalently attached ubiquitin moieties from target proteins, USPs counteract the activity of a relatively small number of E2 enzymes and hundreds of E3 enzymes responsible for specific protein ubiquitination. The subclass of ubiquitin carboxyl-terminal hydrolase enzymes cleaves ubiquitin from small peptides. Deubiquitination serves a number of roles: it protects Lys^{48}-linked polyubiquitinated proteins from targeting to the proteasome and subsequent degradation, but can also control the signaling state characterized by monoubiquitination or Lys^{63}-linked polyubiquitination (1).

Human USP7 was shown to stabilize p53 and, as a consequence, affect cell viability and apoptosis. Initial observations suggested that USP7 stabilizes p53 by direct binding and deubiquitination of p53 (2, 3). Subsequently, USP7 was also demonstrated to deubiquitinate the murine double minute 2 homolog protein, the E3 ubiquitin ligase that targets p53 for proteasomal degradation. The total absence of USP7 destabilized murine double minute 2 homolog, causing an indirect stimulation of p53 protein stability (4, 5). The balance in deubiquitination of these two targets might determine the net outcome of both opposing actions. If the flexibility in target recognition by USP7 is exemplary for the whole USP protein family, unraveling USP-regulated ubiquitin signaling and USP target specificity will prove a challenging task.

A first structural view on the action of USPs was provided by the crystal structure of the USP7 catalytic domain in complex with a covalently attached ubiquitin aldehyde that specifically inhibits USP enzymes (3). The ubiquitin moiety is recognized by an extended protein surface, and its carboxyl-terminal region contacts a narrow groove containing the conserved catalytic triad His, Cys, and Asp. The ubiquitin carboxyl terminus, normally covalently bound to a ubiquitinated target, is positioned at the end of this catalytic channel, which permits binding of the substrate protein by other USP subdomains or by the catalytic core domain itself.

All USPs contain a conserved catalytic domain but vary in both the number and type of subdomains surrounding it (6). In USP7, such subdomains were demonstrated to participate in target recognition. A domain carboxyl-terminal to the USP7 catalytic domain interacted with herpesvirus-infected cell protein 0 (7). Amino-terminal residues were shown to bind p53 (3) and the Epstein-Barr virus nuclear antigen 1 (7). The crystal structure of this amino-terminal domain in complex with an Epstein-Barr virus nuclear antigen 1 peptide shows that the extended target peptide binds to the edge of a β-sandwich (8). Because Epstein-Barr virus nuclear antigen 1 and p53 compete for binding to similar residues in the amino-terminal domain of USP7, Epstein-Barr virus nuclear antigen 1 binding could indirectly destabilize p53 and prevent apoptosis (8).

Subdomains present in multiple USPs include the DUSP domain, the UBP Zinc-finger (ZnF-UBP), and the ubiquitin-interacting motif (9). In at least seven human USPs, single or tandem DUSP domains are located both amino- and carboxyl-terminal to the catalytic core domain (Fig. 1*a*). The DUSP containing the USP family was shown to deubiquitinate or interact with proteins as diverse as the Von Hippel-Lindau tumor suppressor protein (pVHL), the hypoxia-inducible transcription factor HIF-1A, the breast cancer 2 gene product BRCA2, COP9-signalosome-associated cullin E3 ligase complexes, and the thyroid hormone-activating enzyme D2. In a structural genomics effort within our group, we have screened for conserved human protein domains that were suitable for semi-automatic structure elucidation by NMR spectroscopy (10). To identify domains with new folds, we have eliminated those showing significant sequence homology to proteins with a structure deposited in the Protein Data Bank. The amino-terminal DUSP domain of human USP15, a protein recently implicated in COP9 signalosome regulation (11), proved to be a target ideal in terms of spectral dispersion, protein

* This work was supported by the EU SPINE (Structural Proteomics in Europe) Grant QLG2-CT-2002-00988. The costs of publication of this article were defrayed in part by the payment of page charges. This article must therefore be hereby marked "*advertisement*" in accordance with 18 U.S.C. Section 1734 solely to indicate this fact.

The atomic coordinates and structure factors (code 1W6V) have been deposited in the Protein Data Bank, Research Collaboratory for Structural Bioinformatics, Rutgers University, New Brunswick, NJ (http://www.rcsb.org/).

[1] Both authors contributed equally to this work.

[2] Present address: Max-Planck Institute für Entwicklungsbiologie, Spemannstrasse 35/I, D-72076 Tübingen, Germany.

[3] To whom correspondence should be addressed: Dept. of NMR Spectroscopy, Bijvoet Ctr. for Biomolecular Research, Utrecht University, Padualaan 8, 3584 CH Utrecht, The Netherlands. Tel.: 31-30-2532652; Fax: 31-30-2537623; E-mail: g.folkers@chem.uu.nl.

[4] The abbreviations used are: USP, ubiquitin-specific protease; BRCA2, breast cancer 2 gene; CSN, COP9 signalosome; DUSP, domain present in ubiquitin-specific proteases; E2, ubiquitin carrier protein; E3, ubiquitin-protein isopeptide ligase; HIF, hypoxia-inducible factor; NF, nuclear factor; NOE, nuclear Overhauser effect; NOESY, NOE spectroscopy; VDU, Von Hippel-Lindau protein deubiquitinating enzyme; pVHL, Von Hippel-Lindau protein; RING, really interesting new gene; AB3: α/β tripod.

expression, solubility, and stability under NMR conditions. We have determined its solution structure, which displays a novel AB3 fold comprising a 3-fold α-helical bundle that supports a triple-stranded anti-parallel β-sheet. We have discussed the implications of the DUSP domain structure for its potential function in substrate recognition.

MATERIALS AND METHODS

Protein Expression and Purification—A DNA fragment encoding the amino-terminal 120 amino acid residues of human USP15 was amplified by PCR and cloned into the His tag expression vector pET15B (Novagen) from a self-made cDNA library based on a variety of human tumor cell lines essentially as described previously (10). Recombinant protein expression and isotopic labeling was performed in the *Escherichia coli* strain BL21 DE3 RIL (Stratagene) as described previously (10). The harvested bacteria from 0.5 liters of bacterial culture were lysed in 10 ml of lysis buffer (50 mM Na_2HPO_4/NaH_2PO_4, pH 8.0, 300 mM NaCl, 0.1% Triton X-100, 1 mM phenylmethylsulfonyl fluoride, 1 mM β-mercaptoethanol, and 1% protease inhibitor mixture for His-tagged proteins (Sigma)), frozen/thawed, sonicated on ice (20 bursts of 10 s), and centrifuged (30 min, 30,000 $\times$ *g*, 4 °C). The His-tagged hUSP15 was purified on a nickel-MC POROS column (PerSeptive Biosystems) as described previously (10), buffer-exchanged into 10 mM Tris/BisTris, pH 7.0, and 150 mM NaCl diluted to 30 mM NaCl, loaded on an HS-POROS column (PerSeptive Biosystems), purified in 10 mM Tris/BisTris, pH 7.0, with a 30–300 mM NaCl gradient with elution at ~120 mM NaCl, and buffer-exchanged into 50 mM Na_2HPO_4/NaH_2PO_4 at pH 7.0, 150 mM NaCl. The purified His-hUSP15-(1–120) was concentrated to ~1.5 mM using 3-kDa cutoff Centricon (Amicon) spin concentrators. For NMR samples, 10% D_2O and 0.02% NaN_3 were added. Samples were stable for more than a year.

NMR Spectroscopy—All NMR measurements on U-^{15}N- and U-^{13}C,^{15}N-labeled hUSP15 were performed at 298 K on Bruker Avance spectrometers operating at 700 and 900 MHz. The mostly three-dimensional spectra required for resonance assignment and structure determination were recorded using a standard set of NMR experiments recommended for this purpose (see Ref. 12 and references therein). For backbone assignment using CO, CA, and CB resonances, we recorded sequential (i-1) HNCO and CBCA(CO)NH in combination with bifurcate (i,i-1) HN(CA)CO, HNCA, and HNCACB experiments. All spectra were processed with XWinNMR version 3.5 (Bruker Biospin, Rheinstetten, Germany) and assigned using PASTA (13) and SPARKY[5] software. Side chain assignment was obtained from HBHA(CO)NH, HN(CA)HA, (H)CCH-COSY, and H(C)CH-TOCSY spectra, complemented by a two-dimensional H,H-TOCSY with H(^{15}N) suppression in the direct dimension (15) for aromatic moieties. NOE distance restraints were derived from three-dimensional H,NH-NOESY, H,CH-NOESY, and (H)C,NH-NOESY spectra (16) complemented by a two-dimensional H,H-NOESY.

NOE Analysis and Structure Calculations—Automatic NOE assignment and structure calculations were performed using the CANDID module of the program CYANA (17). The first CANDID run was performed when the completeness of proton resonance assignments reached 92%, excluding the first 21 residues in the His tag. The quality of the structures was improved in an iterative procedure, where CANDID runs were followed by manual analysis using the NOE spectra and the preliminary structures to assign missing resonances and improve the quality of the peak lists. Hydrogen bond restraints were defined when consistent with the secondary chemical shifts, expected NOE contacts, and the structures. Manual NOE peak assignments were generally not fixed in the CANDID runs but used to create accurate spectrum-specific chemical shift lists to check the consistency of subsequent CANDID runs and to check the manual assignments. The assignment completeness for the final run was 99% for non-labile protons. The set of 20 structures calculated by CANDID was subjected to water refinement in crystallography NMR software (18) following the standard RECOORD protocol (19). NOE restraints for the water refinement were taken from the sixth cycle of the final CANDID run, because CANDID retains only unambiguous restraints in the final seventh cycle. Dihedral restraints for 47 residues, generated by TALOS on the basis of backbone atom chemical shifts, were included. The structure was validated using WHATCHECK (20) and PROCHECK (21). Structural coordinates were deposited in the Protein Data Bank under accession code 1W6V. NMR assignments were deposited under BioMagResBank entry 6901.

RESULTS

The DUSP Domain Forms an AB3 Tripod—The DUSP domain present in the human USP4, USP11, USP15, USP20, USP32, USP33, and USP48 (Fig. 1*a*) was originally derived from sequence homology (9). The amino acid sequences of several representative DUSP family members, including all reported human DUSP domains, are aligned in Fig. 1*d*. The solution structure of the amino-terminal 120 amino acids of hUSP15 (hereafter referred to as the DUSP domain) was solved by high resolution NMR spectroscopy. Three α-helices formed a bundle supporting a short three-stranded anti-parallel β-sheet in a novel tripod-like AB3 fold (Fig. 1).

Helices α1–α3 are interleaved with strands β1–β3 defining an $\alpha/\beta/\alpha/\beta/\alpha/\beta$ topology (Fig. 1*b*). Helix 2 and β-strand 2 are connected by a long linker that consists of three sub-elements. The highly conserved PGPI motif (Fig. 1*d*, *gold*) is surrounded by loop L1 (*green*) and loop L2 (*magenta*), which vary considerably both in length and sequence (Fig. 1*d*). The PGPI motif packs against the three-helix bundle and is highly ordered (Fig. 1*c*). The backbone root mean square deviation calculated for residues 6–116 is 0.59 $\pm$ 0.11 Å (Table 1). Structural homology searches using DALI, VAST, and MSDfold failed to produce structures with significant homology to the α/β tripod fold of the DUSP domain, indicating it represents a novel fold.

Conserved Residues Participate in Hydrophobic Interactions—The most conserved residues of the DUSP domain, Trp^{37} in α1 and the PGPI motif (P62-I65), interact closely. The PGPI motif wraps around the aromatic side chain of Trp^{37} (Fig. 2*a*) with the hydrophobic side chains of Pro^{62} and Ile^{65} packing against the aromatic ring, which explains the exceptional Ile^{65}-HA chemical shift of 1.33 ppm. The tryptophan HE1 iminoproton is perfectly placed to form a hydrogen bond with the main chain Gly^{63} carbonyl. The Pro^{64} side chain is pointing away from the Trp^{37} aromatic ring, whereas its backbone atoms curve around it in a sharp turn. Although the PGPI motif does not adopt a canonical secondary structure, it is structurally well defined with a low backbone root mean square deviation of 0.53 $\pm$ 0.14 Å.

Isoleucine 65 not only interacts with Trp^{37} but also participates in a second hydrophobic cluster around the conserved Trp^{97} with its γ2-methyl group (Fig. 2*b*). Conserved residues from four structure elements (the PGPI motif, helix α2, strand β2, and the loop preceding strand β3) interact to tie these elements together. The side chains of Tyr^{31} and Pro^{112} pack on one side, and the Ile^{65} methyl γ2 and the Val^{101} side chain pack on the other side of the Trp^{97} indole ring.

Also, the core of the three-helix bundle is stabilized by hydrophobic side chain interactions between conserved residues (Fig. 2*c*). Leucine 100 in helix α3 interacts with α2 residues Phe^{38} and Trp^{41}, of which the

[5] T. D. Goddard and D. G. Kneller, University of California, San Francisco.

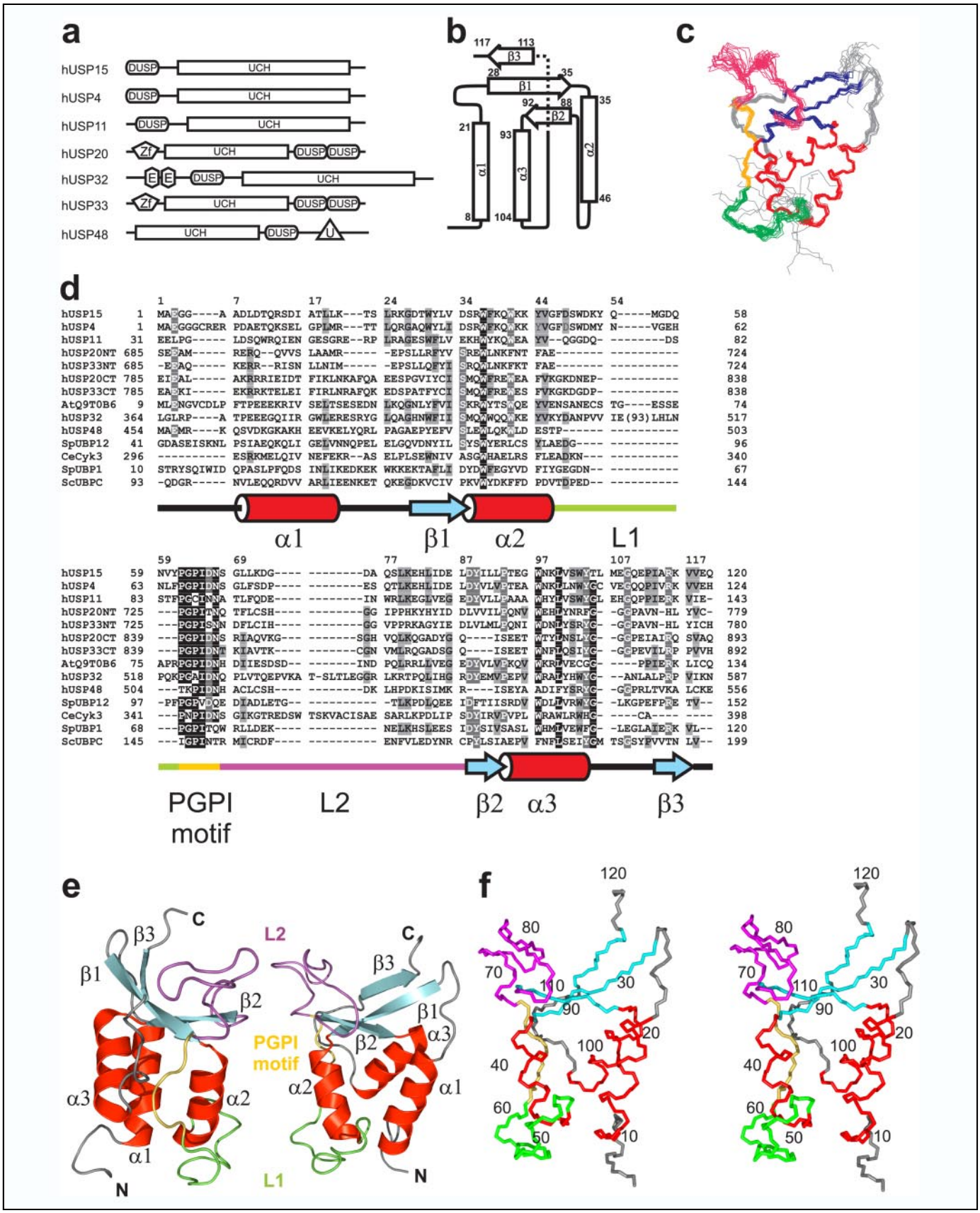

FIGURE 1. **Solution structure of the human USP15 DUSP domain.** *a*, schematic domain organization of human USPs containing DUSP domains: hUSP15 (Swiss Protein Data Base entry Q9Y4E8), hUSP4/Unp (Q13107), hUSP11 (P51784), hUSP20/VDU2 (Q9Y2K6), hUSP32 (Q8NFA0), hUSP33/VDU1 (Q8TEY7), and hUSP48/hUSP31 (TrEMBL entry Q86UV5). *Zf*, zinc finger in USPs; *E*, calcium binding EF-hand; *U*, ubiquitin-like domain. *b*, topology diagram of the hUSP15 DUSP domain, summarizing exact boundaries between secondary structure elements. *c*, ensemble of the 13 lowest energy NMR structures deposited in the Protein Data Bank (1W6V). The backbone traces of the deposited ensemble of NMR structures without

TABLE 1

Structural statistics of the hUSP15 DUSP domain

Unambiguous/ambiguous restraints are listed by range: intraresidual (within the same residue), sequential (between neighboring residues), medium range (between residues 2–4 positions apart), or long range (5 or more amino acids apart). The average root mean square deviation of superimposed backbone and heavy atoms was calculated for the indicated amino acids. Structure Z scores were obtained by WHATCHECK analysis of the deposited ensemble over the whole protein (residues 1–120). The first deposited structure in the ensemble is the structure closest to the ensemble average. The Ramachandran plot was obtained by PROCHECK analysis of backbone torsion angle statistics of the deposited ensemble of the 13 lowest energy structures without nuclear Overhauser effect violations >1.0 Å over the whole protein.

NOE-based distance restraints (unambiguous/ambiguous)	
Intraresidual	577/178
Sequential	623/228
Medium range (2–4)	402/231
Long range (5 or more)	570/359
Total	2172/996
Dihedral restraints	
ϕ/ψ	47/47
Average root mean square deviation to mean (backbone atoms; heavy atoms (Å))	
Overall, amino acids 6–116	0.59 ± 0.11; 1.04 ± 0.09
Structured, amino acids 6–46; 62–68; 88–116	0.49 ± 0.10; 0.95 ± 0.12
Loop L1, amino acids 47–61	0.64 ± 0.22; 1.18 ± 0.34
Loop L2, amino acids 69–87	0.82 ± 0.26; 1.21 ± 0.24
Structure Z scores (WHATCHECK software)	
1st generation packing quality	−1.51 ± 0.14
2nd generation packing quality	−2.22 ± 0.30
Ramachandran plot appearance	−2.62 ± 0.34
χ-1/χ-2 rotamer normality	−1.78 ± 0.35
Backbone conformation	−2.47 ± 0.68
Number of bumps per 100 residues	16.03 ± 3.34
Ramachandran plot (%) (PROCHECK software)	
Most favored regions	86.09 ± 2.64
Allowed regions	11.32 ± 2.87
Generously allowed regions	2.22 ± 0.99
Disallowed regions	0.38 ± 0.63

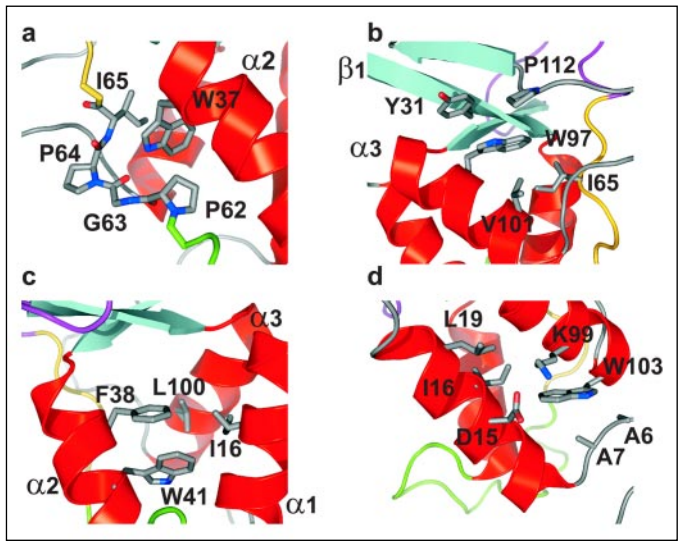

FIGURE 2. **Conserved residues in the DUSP domain participate in hydrophobic interactions.** *a*, the highly conserved PGPI motif wraps around the fully conserved Trp[37] side chain. The backbone trace of amino acids 59–67 and the side chains of Trp[37] and amino acids 62–66 are indicated. *b*, Ile[65] also participates in a hydrophobic cluster around Trp[97] at the interface of the three-helix bundle and the β-sheet. The indicated side chains of Tyr[31] (β2), Val[101] (α3), and Pro[112] (preceding β3) also interact with Trp[97]. *c*, the hydrophobic core of the helical bundle is composed of the highly conserved residue Leu[100] (α3) and side chains from Phe[38] (α2), Trp[41] (α2), and Ile[16] (α1). *d*, the amino-terminal helix (α1) is an integral part of the DUSP domain structure and participates in a network of hydrophobic interactions as indicated.

hydrophobic character is conserved. Helix α1 contributes a non-conserved Ile[16] side chain in USP15 that may be replaced by different residues in other DUSP-containing USP family members.

The DUSP Domain Boundary Definition Should Include an Amino-terminal Helix—When we tried to express soluble protein fragments based on the human USP15 DUSP domain (9), soluble protein was only obtained in high yield after extending the domain amino-terminally to the original DUSP domain boundary definition (amino acids 23–120). Residues 8–21 in this amino-terminal extension form an α-helix (α1) that, despite its low sequence conservation, interacts intimately with the other helices to form the three-helix bundle. The aliphatic side chains of its residues Ile[16] and Leu[19] pack against Lys[99] in helix α3 (Fig. 2*d*). Apart from these hydrophobic interactions, Lys[99] forms a salt bridge with Asp[15] in helix α1 via its protonated amino group. The interface between helices α1 and α3 is further stabilized by hydrophobic interactions between Trp[103], Ala[6], and Ala[7]. These extensive interactions of helix α1 with the other helices underline its vital role in forming the DUSP domain.

DUSP domains have been identified in USPs both at the amino and carboxyl termini and between other subdomains. All amino-terminally located DUSP domains have an extension amino-terminal to the conserved residues in strand β1, previously thought to define the domain boundary. Secondary structure predictions suggest that this extension most likely forms an α-helix, as we observed for the hUSP15 DUSP domain. DUSP domains located carboxyl-terminal to the catalytic core domain also contain such a amino-terminal spacer between the conserved residues of the catalytic and DUSP domains. We therefore expect that all DUSP domains contain the three-helix bundle we observed for hUSP15, despite the low sequence conservation of the amino-terminal helix α1.

Two Variable Loops Flank the PGPI Motif—Interestingly, the most conserved DUSP residues, forming the PGPI motif, are flanked by two long loops that vary both in length and sequence. The length of loop L1, preceding the PGPI motif, ranges from 2 to 110 residues in human DUSP domains, whereas loop L2 ranges from 17 to 32 residues (Fig. 1*d*). The assigned NOEs in these loop regions indicate an inherent absence of canonical secondary structure, yet the root mean square deviation of loops L1 (0.64 ± 0.22 Å) and L2 (0.82 ± 0.26 Å) is only slightly higher than the overall average of 0.59 ± 0.11 Å (Table 1).

The relatively low root mean square deviation in loop L2 is explained by the presence of a hydrophobic cluster formed by leucines 70, 79, and 83 and Tyr[89] in strand β2. Interestingly, although the sequence conservation in loop L2 is very poor, the hydrophobic character of these residues is largely conserved, even in loops of larger and smaller size. Such conservation is not observed in the loop L1 that is missing in hUSP20 and hUSP32, which contain two consecutive DUSP domains (Fig. 1*d*). In these proteins, Pro[83] from the PGPI motif is connected to helix α2 via a small linker of only two residues, which is compatible with the hUSP15 structure.

A Conserved Surface Cluster Is Present at the Loop L2/β-Sheet Interface—A projection of sequence conservation onto the protein surface, shown in Fig. 3, reveals two conserved surface areas that could

NOE violations > 1.0 Å are displayed. Secondary structure elements are indicated by color coding: α-helices (*red*), β-strands (*blue*), loop L1 (*green*), loop L2 (*magenta*), and PGPI motif (residues 62–67, *gold*). *d*, multiple sequence alignment of a representative set of DUSP domains (hUSP15 on *top*). Increasing amino acid identity is indicated by *darker shading*. Gene name abbreviations use *h* (*Homo sapiens*), *At* (*Arabidopsis thaliana*), *Sp* (*S. pombe*), *Sc* (*Saccharomyces cerevisiae*), and *Ce* (*Caenorhabditis elegans*). Secondary structure elements are indicated *below* the sequence and *color-coded* as in *c*. *e*, solution structure of the hUSP15 DUSP domain in two orthogonal views as *ribbon* plot. Secondary structure elements are *color-coded* as in *b*. All pictures were created using PyMol (pymol.sourceforge.net). (46). *f*, stereo representation of backbone trace, *color-coded* as in *b*.

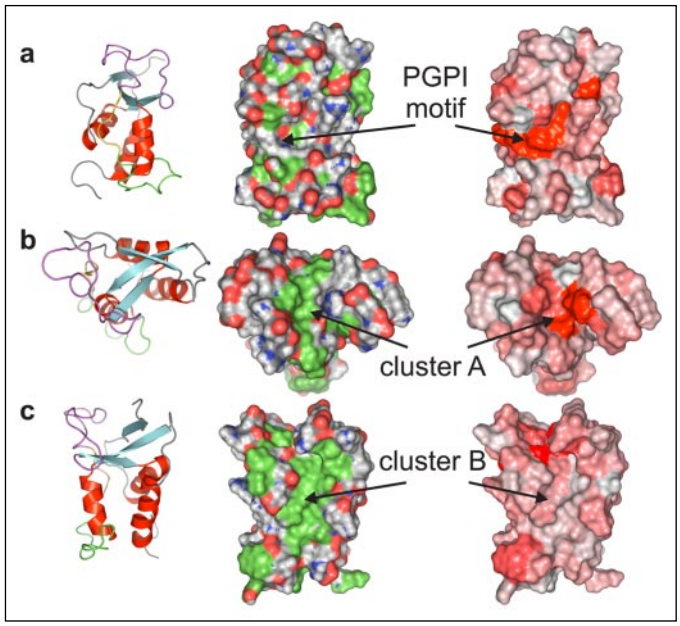

FIGURE 3. **Surface analysis of the hUSP15 DUSP domain.** *Left*, reference *ribbon* diagram *color-coded* as in Fig. 1*c*. *Middle*, surface representation indicating hydrophobic side chains (*green*) and all other atoms in Corey/Pauling/Kultin coloring (carbon, *gray*; hydrogen, *white*; nitrogen, *blue*; oxygen, *red*). *Right*, sequence conservation between the DUSP family members in Fig. 1*a* was calculated using the program ConSurf (47) and displayed on the surface of hUSP15 colored from *white* (not conserved) to *red* (highly conserved). *a*, surface representations of the highly conserved PGPI motif. *b*, the top of the tripod-like fold shows a deep cleft composed of the β-sheet and the loop L2 surface, indicated as *cluster A*. *c*, a shallow, non-conserved hydrophobic cleft between α-helices α1 and α2 is indicated as *cluster B*.

indicate functionally important residues in the DUSP domain. One area contains the PGPI motif, but because the side chains in this motif are mainly buried and wrap around the Trp^{37} aromatic ring, we interpret its role mainly in terms of structural stabilization (Figs. 2*a* and 3*a*). The second conserved area of conservation, cluster A in Fig. 3, contains residues Leu^{32} in β1, Tyr^{89} in β2, β3 residues Ile^{113}, Arg^{115} and Val^{118} and loop L2 residues Leu^{79}, Leu^{83}, and Ile^{84}. Although only Tyr^{89} (β2) and Arg^{115} (β3) are highly conserved residues, the hydrophobicity of the other side chains is conserved as well, producing a largely hydrophobic surface area in a deep cleft at the boundary of the β-sheet and loop L2 (Fig. 3*b*). Conserved hydrophobic surface patches have repeatedly been shown to participate in protein/protein interactions, suggesting that this cluster could play a similar role.

Interestingly, an analysis of surface-exposed hydrophobic side chains reveals another area adjacent to cluster A. This cluster B (Fig. 3*c*), defined by the poorly conserved amino acids Leu^{20} (α1), Leu^{24}, Trp^{30} (β1), Phe^{38} (α2), Phe^{47} (L1), Ile^{90}, and Leu^{91} (β2) forms a second, more shallow cleft of which the hydrophobicity is only conserved in the closest hUSP15 homologs hUSP4 and hUSP11 and to a lesser extent in hUSP32. Clusters A and B together form the most striking surface features of the DUSP domain; both are hydrophobic clefts, one of which is broadly conserved, whereas the other is specific for close hUSP15 relatives.

DISCUSSION

The presented solution structure of the DUSP domain of human USP15 does not show significant homology to any structure so far deposited in the Protein Data Bank, as verified using DALI, VAST, and MSDfold searches. Three interleaved α/β structure repeats form a novel tripod-like AB3 fold with a three-helix bundle and a three-stranded β-sheet resembling the legs and seat of the tripod. Conserved residues are predominantly involved in hydrophobic packing interactions within the three α-helices (Fig. 2). The highly conserved PGPI motif wraps around the fully conserved Trp^{37} side chain in α2 and is flanked by two loops of variable length and sequence composition. The most striking surface feature is a conserved, mainly hydrophobic area in a deep cleft at the interface of loop L2 and the β-sheet.

Although the lack of structural homologs hampers the functional interpretation of the structure, there is experimental data on USPs containing DUSP domains. The best characterized human DUSP containing USPs are the two strongly related USP20 (VDU2) and USP33 (VDU1) that were originally identified as interactors of pVHL (22, 23). pVHL forms an E3 ligase complex with elongins B and C, cullin 2, and the RING finger protein Rbx1 (24). Under normal oxygen conditions, a cage in the pVHL β-domain binds a specific, hydroxylated proline in the hypoxia-inducible transcription factor HIF-1α (25, 26), which results in HIF-1α ubiquitination and degradation. Under low oxygen pressure, the hydroxylation is reversed, causing transcriptional activation of HIF-1α-responsive genes that provide a cellular response to hypoxia. Although both USP20 and USP33 are bound by pVHL and ubiquitinated in a pVHL-dependent fashion, only USP20 can bind HIF-1α and protect it from pVHL-dependent ubiquitination (27). USP20 residues 269–390 are necessary and sufficient for this interaction with HIF-1α, excluding any contribution from the DUSP domains. In contrast, the interaction with pVHL is located within hUSP20 and hUSP33 residues 510–911, including both DUSP domains and part of the catalytic ubiquitin carboxyl-terminal hydrolase catalytic domain (22).

Both hUSP20 and hUSP33 were also demonstrated to bind the iodothyronine deiodinase D2 enzyme that plays a role in thyroid hormone activation. Ubiquitination of D2 can be reversed by both hUSP20 and hUSP33, rescuing the enzyme from proteasomal degradation (28). The interaction with D2 was mapped to the hUSP33 residues 585–786 that comprise a small fragment of the catalytic palm subdomain and the complete first DUSP domain (28). Because the palm fragment is likely unfolded in the absence of the rest of the catalytic domain, the DUSP domain remains the more probable candidate for D2 recognition. Consistent with their participation in the recognition of pVHL and D2 by both hUSP20 and hUSP33, the DUSP domains of both proteins are highly conserved.

In hUSP33 and hUSP20, the amino terminus of the first DUSP domain immediately follows residues homologous to β-strand 14 in the USP7 catalytic domain. The USP7 strand β14 and the carboxyl terminus of the ubiquitin moiety linked to appropriate substrates lie on opposite sides of the catalytic domain, making a contribution to D2 recognition from amino-terminal DUSP residues at the base of the helical bundle seem structurally highly unlikely. The neighboring loop L1 is virtually absent in hUSP20/33, arguing against its participation in D2 recognition. In contrast, the conserved, surface-exposed, and predominantly hydrophobic cleft formed by β-sheet and loop L2 residues (Fig. 3*b*) at over 30 Å of distance from the amino terminus is a more likely candidate for D2 recognition by the hUSP20/33 DUSP domain and for target recognition by DUSP domains in general. Loop L2 forms a clamp-like structure, and the observed sequence variability around residues Leu^{79}, Leu^{83}, and Ile^{84} could contribute to the specificity of such a putative interaction.

hUSP15 itself is catalytically active *in vitro* on a variety of ubiquitin-glutathione *S*-transferase fusions, ubiquitously expressed and highly active in a wide range of cell types (29–32). hUSP15 was observed both in the cytoplasm of NIH3T3 and HeLa cells as well as in HeLa nucleoli (33). Only recently, hUSP15 has been found to co-purify with the human COP9 signalosome (CSN) complex (11) and suggested to be the

human homolog of the *Saccharomyces pombe* Ubp12 protein that regulates the activity of CSN-associated cullin-RING ubiquitin ligases (34, 35). The CSN is a protein complex with many similarities to the proteasome lid that regulates processes as diverse as the cell cycle, transcription, and signal transduction (36–38). The cullin-RING ubiquitin ligase complexes regulated by the CSN recognize substrates for ubiquitination using specific adaptor proteins that are often unstable because of their own cullin-dependent ubiquitination. Ubp12 can inhibit adaptor ubiquitination, which in turn stimulates the ubiquitination and degradation of substrates (34, 35). Similarly, the RING E3 ligase Rbx1 was stabilized by overexpression of human USP15 (11). How hUSP15 and Ubp12 associate with the CSN or recognize their targets remains to be established, but it is intriguing that pVHL and HIF-1α, the binding partners of hUSP20/33, were also shown to interact with the CSN complex and CSN5, respectively (39).

The close hUSP15 homolog hUSP11 was implicated in the regulation of BRCA2 (40). hUSP11 could interact with and deubiquitinate the DNA repair protein BRCA2 and inhibition of hUSP11 expression or inactivation of hUSP11 increased cellular sensitivity to the DNA-damaging agent mitomycin C depending on the presence of BRCA2. Ubiquitination and proteasomal degradation of BRCA2 *in vivo* were nevertheless not affected by hUSP11 mutation or inhibition, suggesting that USP11 might exert its BRCA2-dependent pro-survival function indirectly (40).

Other USP subdomains were previously shown to participate in protein/protein interactions or direct substrate recognition, such as the amino-terminal tumor necrosis factor receptor-associated factor homology domain and a carboxyl-terminal domain of hUSP7 (3, 7, 8), the amino-terminal ZnF-UBP domain of Ubp8 (41), and a Cap-Gly domain in the USP cylindromatosis gene product (42, 43). The cylindromatosis gene product CYLD binds the NFκB essential modulator (43–45) with a contribution by a conserved, surface-exposed hydrophobic cleft (42), similar to the identified DUSP domain cluster A at the loop L2/β-sheet boundary (Fig. 3*b*). Although the catalytic domain in USPs is responsible for the deubiquitination of their targets, the surrounding subdomains confer target specificity in all these examples. Consistent with this general model, the experimental data on pVHL and D2 and the surface properties of the hUSP15 DUSP domain suggest that the DUSP domain in USP enzymes plays a role in protein/protein interaction or direct substrate recognition.

Acknowledgments—We thank Rolf Boelens and Alexandre Bonvin for stimulating discussions and H. van Aken, M. Hilbers, and J. van der Zwan for technical support.

REFERENCES

1. Amerik, A. Y., and Hochstrasser, M. (2004) *Biochim. Biophys. Acta* **1695,** 189–207
2. Li, M., Chen, D., Shiloh, A., Luo, J., Nikolaev, A. Y., Qin, J., and Gu, W. (2002) *Nature* **416,** 648–653
3. Hu, M., Li, P., Li, M., Li, W., Yao, T., Wu, J. W., Gu, W., Cohen, R. E., and Shi, Y. (2002) *Cell* **111,** 1041–1054
4. Li, M., Brooks, C. L., Kon, N., and Gu, W. (2004) *Mol. Cell* **13,** 879–886
5. Cummins, J. M., Rago, C., Kohli, M., Kinzler, K. W., Lengauer, C., and Vogelstein, B. (2004) *Nature* **428,** 1 p following 486
6. Quesada, V., Diaz-Perales, A., Gutierrez-Fernandez, A., Garabaya, C., Cal, S., and Lopez-Otin, C. (2004) *Biochem. Biophys. Res. Commun.* **314,** 54–62
7. Holowaty, M. N., Sheng, Y., Nguyen, T., Arrowsmith, C., and Frappier, L. (2003) *J. Biol. Chem.* **278,** 47753–47761
8. Saridakis, V., Sheng, Y., Sarkari, F., Holowaty, M. N., Shire, K., Nguyen, T., Zhang, R. G., Liao, J., Lee, W., Edwards, A. M., Arrowsmith, C. H., and Frappier, L. (2005) *Mol. Cell* **18,** 25–36
9. Letunic, I., Copley, R. R., Schmidt, S., Ciccarelli, F. D., Doerks, T., Schultz, J., Ponting, C. P., and Bork, P. (2004) *Nucleic Acids Res.* **32,** D142–D144
10. Folkers, G. E., van Buuren, B. N., and Kaptein, R. (2004) *J. Struct. Funct. Genomics* **5,** 119–131
11. Hetfeld, B. K., Helfrich, A., Kapelari, B., Scheel, H., Hofmann, K., Guterman, A., Glickman, M., Schade, R., Kloetzel, P. M., and Dubiel, W. (2005) *Curr. Biol.* **15,** 1217–1221
12. Sattler, M., Schleucher, J., and Griesinger, C. (1999) *Prog. Nucl. Mag. Res. Sp.* **34,** 93–158
13. Leutner, M., Gschwind, R. M., Liermann, J., Schwarz, C., Gemmecker, G., and Kessler, H. (1998) *J. Biomol. NMR* **11,** 31–43
14. Deleted in proof
15. Whitehead, B., Tessari, M., DÃ¼x, P., Boelens, R., Kaptein, R., and Vuister, G. W. (1997) *J. Biomol. NMR* **9,** 313–316
16. Diercks, T., Coles, M., and Kessler, H. (1999) *J. Biomol. NMR* **15,** 177–180
17. Herrmann, T., Guntert, P., and Wuthrich, K. (2002) *J. Mol. Biol.* **319,** 209–227
18. Brunger, A. T., Adams, P. D., Clore, G. M., DeLano, W. L., Gros, P., Grosse-Kunstleve, R. W., Jiang, J. S., Kuszewski, J., Nilges, M., Pannu, N. S., Read, R. J., Rice, L. M., Simonson, T., and Warren, G. L. (1998) *Acta. Crystallogr. Sect. D. Biol. Crystallogr.* **54,** 905–921
19. Nederveen, A. J., Doreleijers, J. F., Vranken, W., Miller, Z., Spronk, C. A., Nabuurs, S. B., Guntert, P., Livny, M., Markley, J. L., Nilges, M., Ulrich, E. L., Kaptein, R., and Bonvin, A. M. (2005) *Proteins* **59,** 662–672
20. Hooft, R. W., Vriend, G., Sander, C., and Abola, E. E. (1996) *Nature* **381,** 272
21. Laskowski, R. A., Rullmannn, J. A., MacArthur, M. W., Kaptein, R., and Thornton, J. M. (1996) *J. Biomol. NMR* **8,** 477–486
22. Li, Z., Na, X., Wang, D., Schoen, S. R., Messing, E. M., and Wu, G. (2002) *J. Biol. Chem.* **277,** 4656–4662
23. Li, Z., Wang, D., Na, X., Schoen, S. R., Messing, E. M., and Wu, G. (2002) *Biochem. Biophys. Res. Commun.* **294,** 700–709
24. Czyzyk-Krzeska, M. F., and Meller, J. (2004) *Trends Mol. Med.* **10,** 146–149
25. Hon, W. C., Wilson, M. I., Harlos, K., Claridge, T. D., Schofield, C. J., Pugh, C. W., Maxwell, P. H., Ratcliffe, P. J., Stuart, D. I., and Jones, E. Y. (2002) *Nature* **417,** 975–978
26. Min, J. H., Yang, H., Ivan, M., Gertler, F., Kaelin, W. G., Jr., and Pavletich, N. P. (2002) *Science* **296,** 1886–1889
27. Li, Z., Wang, D., Messing, E. M., and Wu, G. (2005) *EMBO Rep.* **6,** 373–378
28. Curcio-Morelli, C., Zavacki, A. M., Christofollete, M., Gereben, B., de Freitas, B. C., Harney, J. W., Li, Z., Wu, G., and Bianco, A. C. (2003) *J. Clin. Investig.* **112,** 189–196
29. Angelats, C., Wang, X. W., Jermiin, L. S., Copeland, N. G., Jenkins, N. A., and Baker, R. T. (2003) *Mamm. Genome* **14,** 31–46
30. Baker, R. T., Wang, X. W., Woollatt, E., White, J. A., and Sutherland, G. R. (1999) *Genomics* **59,** 264–274
31. Park, K. C., Choi, E. J., Min, S. W., Chung, S. S., Kim, H., Suzuki, T., Tanaka, K., and Chung, C. H. (2000) *Biochem. J.* **349,** 443–453
32. Ovaa, H., Kessler, B. M., Rolen, U., Galardy, P. J., Ploegh, H. L., and Masucci, M. G. (2004) *Proc. Natl. Acad. Sci. U. S. A.* **101,** 2253–2258
33. Soboleva, T. A., Jans, D. A., Johnson-Saliba, M., and Baker, R. T. (2005) *J. Biol. Chem.* **280,** 745–752
34. Wee, S., Geyer, R. K., Toda, T., and Wolf, D. A. (2005) *Nat. Cell Biol.* **7,** 387–391
35. Zhou, C., Wee, S., Rhee, E., Naumann, M., Dubiel, W., and Wolf, D. A. (2003) *Mol. Cell* **11,** 927–938
36. Li, L., and Deng, X. W. (2003) *Trends Cell Biol.* **13,** 507–509
37. Schwechheimer, C. (2004) *Biochim. Biophys. Acta* **1695,** 45–54
38. Wolf, D. A., Zhou, C., and Wee, S. (2003) *Nat. Cell Biol.* **5,** 1029–1033
39. Bemis, L., Chan, D. A., Finkielstein, C. V., Qi, L., Sutphin, P. D., Chen, X., Stenmark, K., Giaccia, A. J., and Zundel, W. (2004) *Genes Dev.* **18,** 739–744
40. Schoenfeld, A. R., Apgar, S., Dolios, G., Wang, R., and Aaronson, S. A. (2004) *Mol. Cell. Biol.* **24,** 7444–7455
41. Ingvarsdottir, K., Krogan, N. J., Emre, N. C., Wyce, A., Thompson, N. J., Emili, A., Hughes, T. R., Greenblatt, J. F., and Berger, S. L. (2005) *Mol. Cell. Biol.* **25,** 1162–1172
42. Saito, K., Kigawa, T., Koshiba, S., Sato, K., Matsuo, Y., Sakamoto, A., Takagi, T., Shirouzu, M., Yabuki, T., Nunokawa, E., Seki, E., Matsuda, T., Aoki, M., Miyata, Y., Hirakawa, N., Inoue, M., Terada, T., Nagase, T., Kikuno, R., Nakayama, M., Ohara, O., Tanaka, A., and Yokoyama, S. (2004) *Structure* (*Camb.*) **12,** 1719–1728
43. Kovalenko, A., Chable-Bessia, C., Cantarella, G., Israel, A., Wallach, D., and Courtois, G. (2003) *Nature* **424,** 801–805
44. Brummelkamp, T. R., Nijman, S. M., Dirac, A. M., and Bernards, R. (2003) *Nature* **424,** 797–801
45. Trompouki, E., Hatzivassiliou, E., Tsichritzis, T., Farmer, H., Ashworth, A., and Mosialos, G. (2003) *Nature* **424,** 793–796
46. Deleted in proof
47. Landau, M., Mayrose, I., Rosenberg, Y., Glaser, F., Martz, E., Pupko, T., and Ben-Tal, N. (2005) *Nucleic Acids Res.* **33,** W299–W302